

Staircase Recognition and Location Based on Polarization Vision

Weifeng Kong^{1,2}, Zhiying Tan^{1,*}

Abstract—Staircase is one of the most common structures in artificial scenes. However, it is difficult for humanoid robots and people with lower limb disabilities or visual impairment to cross the scene without the help of sensors and intelligent algorithms. Staircase scene perception technology is a prerequisite for recognition and localization. This technology is of great significance for the mode switching of the robot and the calculation of the footprint position to adapt to the discontinuous terrain. However, there are still many problems that constrain the application of this technology, such as low recognition accuracy, high initial noise from sensors, unstable output signals and high computational requirements. In terms of scene reconstruction, the binocular and time of flight (TOF) reconstruction of the scene can be easily affected by environmental light and the surface material of the target object. In contrast, due to the special structure of the polarizer, the polarization can selectively transmit polarized light in a specific direction and this reconstruction method relies on the polarization information of the object surface. So the advantages of polarization reconstruction are reflected, which are less affected by environmental light and not dependent on the texture information of the object surface. In this paper, in order to achieve the detection of staircase, this paper proposes a contrast enhancement algorithm that integrates polarization and light intensity information, and integrates point cloud segmentation based on YOLOv11. To realize the high-quality reconstruction, we proposed a method of fusing polarized binocular and TOF depth information to realize the three-dimensional (3D) reconstruction of the staircase. Besides, it also proposes a joint calibration algorithm of monocular camera and TOF camera based on ICP registration and improved gray wolf optimization algorithm. Finally, the recognition network can achieve an accuracy of 98.7%. The joint calibration algorithm can achieve a calibration accuracy of 0.33mm, which is higher than the traditional binocular calibration algorithm. At the distance of 0.5m, the reconstruction error of this algorithm is less than 0.2%, and finally the orientation information of the staircase is obtained on the reconstructed point cloud.

Keywords—Staircase recognition; Polarization - TOF fusion; Polarization ambiguity correction; Joint calibration

I. INTRODUCTION

As a general scenario, the staircase interferes with the traversal of humanoid robots, lower limb disabilities, or visually impaired individuals due to its special physical structure. Accurate staircase recognition technology is a prerequisite for navigation and control, and staircase recognition technology has attracted the attention of many scholars [1],[2],[3]. Staircase recognition is of great significance for the mode switching and foothold position calculation of robots, which can improve the overall performance of robots in stair scenes. As a common terrain, stairs are very difficult for humanoid robots and people with lower limb disabilities or visual impairments. Therefore, it is of great significance to design a staircase scene perception algorithm.

At present, the staircase recognition is mainly applied in the fields of rehabilitation medicine and humanoid robots. Because accurate gait control is one of the prerequisites for normal gait, while gait disorders can lead to cessation of movement, falls, and increased mortality [4]. The accurate recognition of human gait requires the joint action of sensors and signal processing algorithms [5], and the signals collected by sensors are processed and feedback adjusted through the upper computer [6]. This technology can provide auxiliary guidance to target populations, such as visual navigation systems for blind individuals and gait monitoring for Parkinson's patients. The sensors used for staircase recognition are mainly divided into wearable sensors and photoelectric sensors. Wearable sensors include inertial measurement units, electromyographic sensors,

etc. They are mainly aimed at recognizing the intention of movement in staircase scenes. The signals collected by the sensors are processed by classification algorithms or neural networks to achieve the classification of motion intentions, thereby achieving the goal of indirect scene recognition [7]. Photoelectric sensors include monocular camera, depth camera, radar and so on, which are mainly used for scene recognition before entering the staircases. Staircase recognition is very important in robot motion navigation and control, so it is necessary to recognize the staircase, but the existing algorithms have the problems of low recognition accuracy, slow running speed and unable to achieve scene versatility [8].

However, in order to make the motion function of the robot more perfect, the 3D reconstruction of the staircase based on the recognition results is indispensable. Nowadays, a large number of sensors are widely used in the 3D reconstruction of the scene, but these sensors have the characteristics of poor imaging details, low imaging accuracy and efficiency. For example, line structured light cannot achieve single-frame shape recovery because its projection pattern is a straight line, resulting in low efficiency [9]. The projected structured light is easily affected by reflection, illumination and other reasons, and the encoded information is lost in some areas. Depth camera and radar are limited by factors such as time resolution, environment, and multipath effects [10]. The multipath effect of depth sensor data is shown in Fig.1, which causes discontinuous depth regions in the depth map, resulting in errors in depth measurement. To solve this problem, a multi-sensor fusion method is introduced to fuse polarization and TOF for 3D reconstruction of staircase.

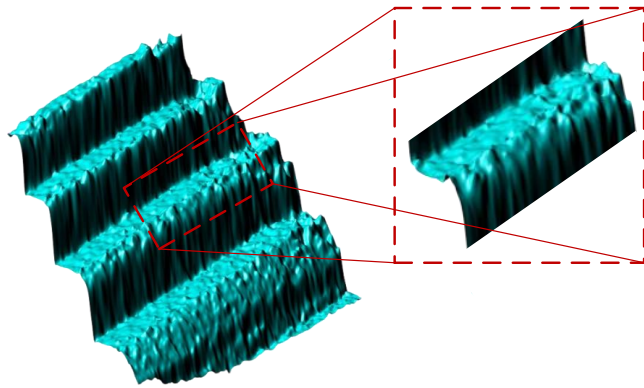


Fig.1 Schematic diagram of multipath effect in depth sensor data

Polarization imaging can obtain more multi-dimensional information besides the ordinary intensity information [11]. Reflection of unpolarized light by the surface of an object changes the polarization of the light, and the polarization of the light reflected from the object conveys information about the material properties and shape of the object. 3D reconstruction can be carried out by detecting the degree of polarization (DoP) and polarization angle of the object surface. Polarization 3D reconstruction technology has the advantages of simple imaging equipment, easy to implement algorithm, rich reconstruction details and so on, so polarization 3D reconstruction technology has important research significance [12]. However, there are a series of problems, such as the ambiguity of the azimuth angle and the inability to obtain the real 3D information of the object [13], [14], [15], [16], which are studied in this paper. To solve these problems, here we introduce the method of binocular vision and TOF. Compared with depth camera, radar and monocular camera, binocular vision can simultaneously obtain the appearance image and three-dimensional information of an object. It can not only utilize the geometric features of the object, but also analyze and correct the ambiguity of the polarization gradient field by combining its visual features such as texture and color, providing more comprehensive and rich information. However, data holes are inevitable in the stereo matching process [17]. Although the TOF method is affected by multipath effects, it can obtain full pixel

reconstruction [18]. Therefore, combining the two methods, this paper uses binocular to correct polarization ambiguity and TOF to correct binocular hole regions. Their complementary advantages not only correct ambiguity, but also effectively avoid data hole regions. However, the fusion of multiple sensors will face the problem of sensor calibration, which is also a key focus of this paper. So far, there has been no reconstruction using binocular polarization and TOF fusion internationally.

To sum up, in order to establish an object detection model and address the azimuth ambiguity in polarization 3D reconstruction, several methods are proposed this paper proposed:

(1) A staircase detection method based on polarization information fusion and 2D-3D fusion is proposed, which significantly enhances image contrast through feature level fusion of DoP image and intensity image. At the same time, depth camera assisted recognition is used to further improve the detection accuracy and robustness of staircase.

(2) Joint calibration of monocular and TOF cameras. Since polarization camera and TOF camera have different resolutions, so the traditional binocular calibration algorithm cannot be applied in this condition. We proposed a joint calibration algorithm combined with the improved joint grey wolf optimization algorithm for ICP algorithm.

(3) Polarization gradient field ambiguity correction with binocular and TOF. Firstly, a three-dimensional shape similar to the surface of the target object is reconstructed by a binocular vision method, and a relatively accurate gradient field is obtained, which is used as a reference to correct the ambiguity problem in the polarization gradient field. Due to the existence of data holes in the binocular stereo matching process, the polarization gradient field corresponding to this part of the region has not been effectively corrected, and the TOF depth information is introduced to correct it.

II. STAIRCASE DETECTION BASED ON POLARIZATION INFORMATION FUSION AND 2D-3D FUSION

In the motion of robot staircase scenes, real-time reconstruction of the environment requires a large amount of computing resources. In order to save computing power, the staircase can be recognized to determine the ROI area of the staircase in the field of view, and then trigger scene reconstruction. Reconstructing scenes within local ROI regions not only avoids the consumption of computing resources, but also improves real-time performance.

In object detection tasks, the reflection on the surface of the target object is one of the key factors affecting detection accuracy. Reflection can cause abnormal enhancement of pixel intensity in the target region, thereby disrupting the texture and edge information of the image and reducing the contrast between the target and the background. This makes it difficult for object detection models to accurately distinguish between target and non-target regions, thereby reducing the accuracy and robustness of detection.

The DoP image is an image generated by measuring the polarization state of light. It can effectively capture the polarization information of the target surface, highlight the texture and edge features of objects, and simultaneously suppress the reflective regions, thereby enhancing the contrast and detectability of the image. The DoP image can be calculated from images I_0 , I_{45} , I_{90} , and I_{135} using the Stokes method. When the polarization angles are 0° , 45° , 90° , and 135° , respectively. DoP can be expressed as:

$$\rho = \frac{\sqrt{s_1^2 + s_2^2}}{s_0} \quad (1)$$

Among them, $s_0 = (I_0 + I_{45} + I_{90} + I_{135}) / 4$, $s_1 = I_0 - I_{90}$, $s_2 = I_{45} - I_{135}$.

The intensity image intuitively displays the distribution of light intensity and can clearly present the contours, shapes, and general surface features of objects. To address the issue of reflection, this paper proposes a fusion strategy for the DoP image and the intensity image based on a Multilayer Perceptron

(MLP). By integrating these two maps, the detailed information provided by the DoP image, such as microstructure, can be incorporated into the overall contour of the intensity image. This allows us to grasp the overall shape of the object while also observing its fine details, thereby obtaining richer and more comprehensive image information.

The structure of the DoP and intensity image fusion network is shown in Fig.2, which is located at the input of YOLOv11. Convolution operations are first performed on the data of the two channels, namely the DoP and the intensity image, to extract local features and enhance the feature representation. Subsequently, the data from the two channels after convolution processing are concatenated at the element level to form an integrated feature vector, effectively fusing the information of polarization and intensity, and providing a more comprehensive feature representation for subsequent analysis. This feature vector is then input into a Multilayer Perceptron (MLP) network for training and learning. Leveraging its powerful feature learning capabilities, the MLP network can automatically identify features and patterns in the data and output two weights, DoP_{weight} and I_{weight} , corresponding to the importance of the DoP image and the intensity image in the fusion process, respectively. Finally, these two weights are multiplied element-wise with the original DoP image and the intensity image, respectively, and the results are added together to achieve image fusion. The final fused image can be represented as:

$$I_{final} = DoP_{weight} * P + I_{weight} * I \quad (2)$$

Where, P and I represent DoP image and intensity image, respectively.

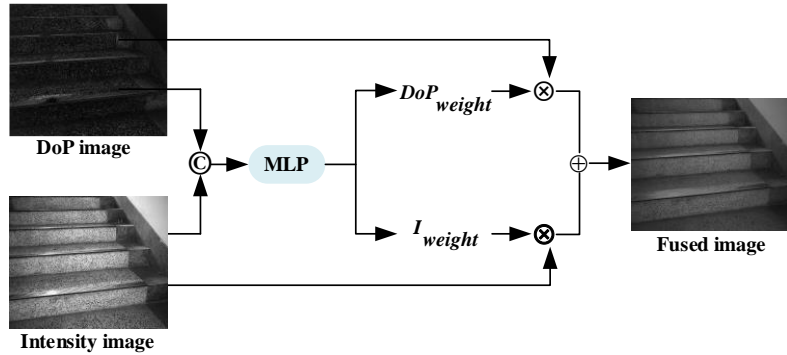


Fig.2 Polarization and intensity image fusion based on MLP network

This weighted fusion method fully considers the characteristics of the two images: the DoP image can effectively capture the polarization information of the target surface, while the intensity map retains the brightness information of the original image. Through the non-linear mapping capability of the MLP network, the fusion of these two types of image information at the feature level significantly enhances the contrast of the fused image.



Fig.3 Recognition mistake

Although the optimized YOLOv11 model has shown satisfactory performance in practical applications, recognition errors are still inevitable. As shown in Fig.3, the model encountered a misjudgment when

distinguishing between upstairs and downstairs, mistakenly identifying the scene upstairs as downstairs. In order to improve the robustness and accuracy of the algorithm, this paper proposes a method of using depth camera to assist recognition. Depth camera can capture the 3D geometric information of objects in the scene, thus providing more abundant and accurate data for going up and down stairs. By combining the depth camera data, we can verify or correct the recognition results of YOLOv11. The staircase point cloud is divided into vertical and horizontal planes by using the difference of normal differences, and further recognition analysis is carried out according to the probability distribution of the two planes.

According to the characteristics of most stairs, they are similar to those in Fig.4. The horizontal planes are labeled "1", "2", "3", and the vertical planes are labeled "a", "b", "c". Theoretically, there is a normal line perpendicular to the surface as shown in Fig.4. This structure motivates us to segment the staircase surface by KD-Tree Euclidean clustering according to the distribution of normal vectors \tilde{n}_1 and \tilde{n}_2 on the vertical and horizontal planes of the staircase surface, which is inspired by the difference of the direction of the normal vector of the staircase surface.

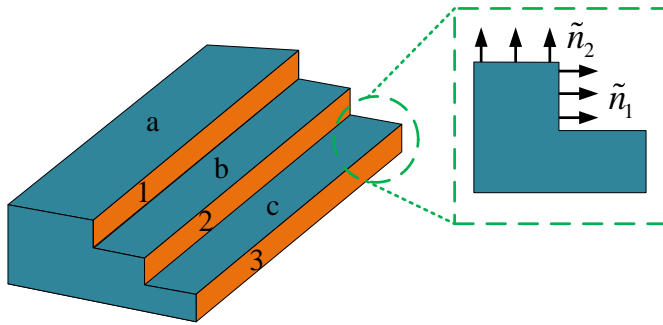


Fig.4 Schematic diagram of stairs

In our strategy, as shown in Algorithm 1, if the deep learning identifies that the results of the previous and next frames are different, the depth camera is triggered to collect the point cloud data of the scene. Since YOLOv11 has previously identified and obtained the ROI region of interest. Therefore, the processing and calculation of the point cloud can be performed in the local region of the ROI.

Algorithm 1 Staircase scene recognition combined with point cloud

Input: Front frame recognition result F , back frame recognition result B and point cloud segmetion result P .

Output: Accurate recognition results I .

```

1: if  $B = F \wedge B \neq \emptyset \wedge F \neq \emptyset$  then
2:    $I \leftarrow B$ ; // Step 1. Check whether the results of the frames front and back are consistent
3: else if  $P = F$  then
4:    $I \leftarrow F$ ; // Step 2. Due to the inconsistency between the results of front and back the
   frames, the point cloud segmentation result is consistent with the front frame, therefore
   the output result is the result of the front frame
5: else
6:    $I \leftarrow B$ ;
7:end if
8:return  $I$ ;
```

In order to speed up the algorithm and avoid the interference of non-target objects, Image processing calculations were performed on regions of interest previously obtained with YOLOv11. After the staircase point cloud is segmented in the region of interest, if the proportion of the total number of vertical plane point clouds L_1 and the total number of horizontal plane point clouds L_2 to the total number of point clouds L in the region of interest is greater than the set threshold T_1 , it is going upstairs. Similarly, if the proportion of the horizontal plane is greater than the set threshold T_2 , it can be judged as going downstairs, as shown in

Eq. (3). In this paper, T_1 and T_2 are 0.4 and 0.8, respectively. At this point, the further detection is completed, and finally the detection of the terrain is completed.

$$\begin{cases} \frac{L_1}{L} > T_1, \frac{L_2}{L} > T_1 & \text{upstairs} \\ \frac{L_2}{L} > T_2 & \text{downstairs} \end{cases} \quad (3)$$

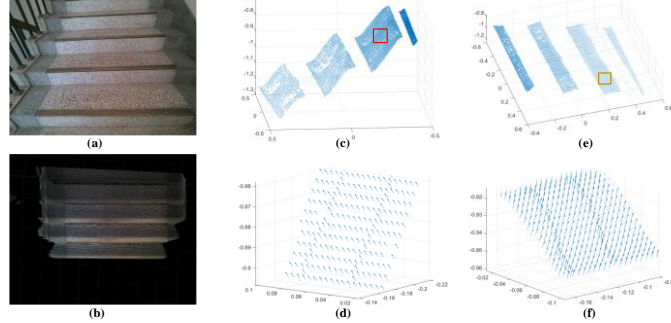


Fig.5 Diagram of point cloud segmentation:(a) Monocular image; (b) Original point cloud; (c) Horizontal planes segmentation result; (d) Local enlarged view of the normal distribution in horizontal planes; (e) Vertical planes segmentation result; (f) Local enlarged view of the normal distribution in vertical planes

The method of point cloud segmentation has been tested for 300 times on the point cloud obtained by the depth camera. The plane is segmented according to the difference of the normal shown in Fig.5. The accuracy of this method can reach 96.7%. Therefore, this method is suitable for further detection. On the basis of the 97.1% recognition accuracy of the YOLOv11 model, the introduction of 3D depth information as redundant information can reduce false recognition and improve the recognition accuracy to 98.7%.

III. STAIRCASES RECONSTRUCTION USING BINOCULAR POLARIZATION AND TOF FUSION

In the aspect of 3D reconstruction of the scene, polarization 3D reconstruction is used in this section. This method relies on the polarization information of the target object, so polarization 3D reconstruction has low requirements for the reconstructed object and does not depend on the texture details of the object surface. Therefore, it can realize the 3D reconstruction of low-texture target objects and is less affected by illumination. However, it has the problem of the ambiguity of the polarization information. To solve this problem, here we introduce binocular polarization and TOF fusion to reach the high-quality reconstruction. In the process of the fusion, the calibration relationship between sensors is crucial.

A. Joint calibration of monocular and TOF cameras

In the traditional dual target positioning algorithm, P is a point in the common field of view of the left and right cameras. The ultimate goal of binocular calibration is to obtain the transfer matrix between the left and right cameras.

Before the fusion of TOF and polarization camera for 3D reconstruction, the relative pose relationship between the two cameras needs to be calculated. In this scheme, the resolution of the TOF camera is 640×480 , and the resolution of the monocular polarization camera is 1224×1024 , so the traditional binocular calibration method has limitations on this. The images captured by polarization and TOF camera are shown in Fig.6. To solve this problem, this paper proposes a joint calibration method combining ICP registration and gray wolf optimization algorithm. The ICP registration algorithm is a 3D point cloud matching algorithm, assuming that there are two groups of point clouds to be registered, namely, the source point cloud $\mathcal{P} = \{p_1, p_2, \dots, p_n\}$ to be matched and the target point cloud $\mathcal{Q} = \{q_1, q_2, \dots, q_n\}$ to be finally

matched. The transformation matrix between the two sets of point clouds is calculated by the registration algorithm, and the ultimate goal is to minimize the error function after registration. The error function can be expressed as:

$$E(\mathbf{R}, \mathbf{T}) = \frac{1}{n} \sum_{i=1}^n \left\| \mathbf{q}_i - (\mathbf{R}\mathbf{p}_i + \mathbf{T}) \right\|^2 \quad (4)$$

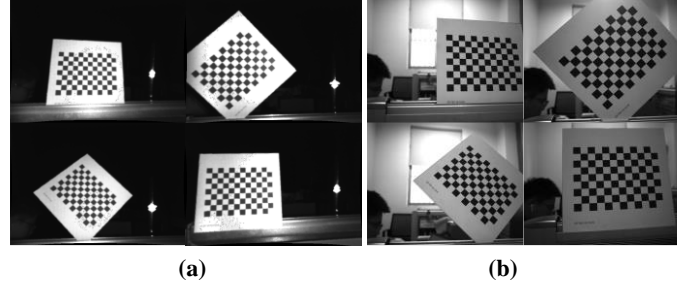


Fig.6 Part of the images of calibration board: (a) Images captured by TOF camera; (b) Images captured by polarization camera

In order to avoid the inaccurate results caused by the ICP algorithm falling into the local minimum or the errors of the two original point clouds, which ultimately affect the registration results between the source point cloud and the target point cloud, the checkerboard calibration board is used in this paper to combine the ICP registration and the gray wolf optimization algorithm for joint calibration. The steps of joint calibration are as follows:

(1) a polarization camera and a TOF camera are rigidly and fixedly connected, a calibration plate is placed in the common visual field of the polarization camera and the TOF camera, images of the calibration plate are collected at the same time, and 20 groups of images are taken;

(2) According to the internal reference data of the camera and the world coordinate system of the corner point of the calibration board, the pose of the calibration board can be estimated to obtain the rotation and translation matrix of the calibration board under the camera coordinate system, and the world coordinate of the chessboard corner point is converted and calculated to obtain the 3D point cloud data of the corner point under the camera coordinate system. The point cloud obtained by the TOF camera is $\mathbf{P} = \{\mathbf{p}_1, \mathbf{p}_2, \dots, \mathbf{p}_n\}$, the point cloud obtained by the polarization camera is $\mathbf{Q} = \{\mathbf{q}_1, \mathbf{q}_2, \dots, \mathbf{q}_n\}$. The initial transformation rotation matrix \mathbf{R} and the translation vector \mathbf{T} of the relative pose relationship between the polarization camera and the TOF camera are calculated by Zhang's calibration method for the ICP registration algorithm.

(3) Based on the relative pose relationship between the polarization camera and the TOF camera obtained from the dual objective method, the initial values for ICP registration are iteratively solved to obtain the relatively accurate pose relationship between point clouds \mathbf{P} and \mathbf{Q} ;

(4) In order to avoid the defect of ICP algorithm easily falling into local optima and ultimately leading to inaccurate matching results, the grey wolf optimization algorithm is used to further optimize the fitness function of Eq. (4) for the matching results.

The grey wolf optimization algorithm is a bionic optimization algorithm, which refers to the hierarchical system and some habits of hunting behavior in the grey wolf population, and has the advantages of simple parameters and easy implementation [20]. The optimization process of the algorithm can be divided into two stages. In the early stage, the core task of global search is to initially lock the region where the global optimal solution is most likely to appear. In order to achieve this goal, we need to ensure that the search range covers the whole search space and prevent any potential optimal solution candidates from being missed, so as to locate the optimal solution more accurately. In the later stage of local search, it focuses on carrying out small-

scale fine search near the location determined by global search. This step aims to further refine the position of the optimal solution obtained by global search, so as to obtain a more accurate solution.

The grey wolf population has a strict hierarchy, and the behavior of the population is also reflected in the gray wolf optimization algorithm. Suppose there are three gray wolves in the wolf pack, which are marked as wolf α , wolf β and wolf δ respectively. Among them, wolf α has a higher level of status, which determines the behavior of the wolf pack to the greatest extent. In each position update process, the grey wolf position updated in the previous update will be used as a reference. In the d -dimensional search space, the position of the k -th grey wolf individual at the t -th iteration is denoted as $X_k(t)$, and this position update mechanism helps the grey wolf group to gradually approach the optimal solution in the search space. The mathematical model of grey wolf tracking prey can be expressed as:

$$D = |CX_p(t) - X_k(t)| \quad (5)$$

$$X_k(t+1) = X_p(t) - AD \quad (6)$$

Where Eq. (5) is the expression for the search step, $X_p(t)$ represents the current position of the prey, and $X_k(t+1)$ represents the updated position of the current individual. In addition, A and C play a key role in the algorithm as disturbance factors, which are defined as follows:

$$A = 2a \cdot \text{rand}() - a \quad (7)$$

$$C = 2 \cdot \text{rand}() \quad (8)$$

Where $\text{rand}()$ is a random number between $[0,1]$, a is the convergence factor defined as:

$$a = 2 \times (1 - \frac{t}{T}) \quad (9)$$

Where, T is the total number of iterations. The position update formula of wolf α , wolf β and wolf δ of the population individuals is:

$$\begin{cases} D_\alpha = |C_1 X_\alpha(t) - X_k(t)| \\ D_\beta = |C_2 X_\beta(t) - X_k(t)| \\ D_\delta = |C_3 X_\delta(t) - X_k(t)| \end{cases} \quad (10)$$

$$\begin{cases} X_1(t+1) = X_\alpha(t) - A_1 D_\alpha \\ X_2(t+1) = X_\beta(t) - A_2 D_\beta \\ X_3(t+1) = X_\delta(t) - A_3 D_\delta \end{cases} \quad (11)$$

$$X_k(t+1) = \frac{1}{3} \sum_{i=1,2,3} X_i(t+1) \quad (12)$$

Among them, $X_\alpha(t)$, $X_\beta(t)$ and $X_\delta(t)$ respectively represent the current position of wolf α , wolf β and wolf δ . D_α , D_β and D_δ correspond to the search steps of the three-headed wolf, and they determine the movement distance of different wolf in the search process. $X_i(t+1)(i=1,2,3)$ represents the position of the individual grey wolf after the guidance update of wolf α , wolf β and wolf δ . $A_i(i=1,2,3)$ and $C_i(i=1,2,3)$ are the perturbation factors of Eq. (7)-(8).

In the grey wolf optimization algorithm, it can be seen from Eq. (12) that the position of the next movement of the population needs to be jointly decided by wolf α , wolf β and wolf δ . The role of the three wolves in updating the position of the movement is the same, but this decision-making method cannot reflect the guidance and importance of the three wolves to the decision-making of the group leaders. In order to realize the self-adaptive adjustment of the weight proportion of the decision-making individual in different periods,

in each iterative calculation process of the algorithm, the dynamic weight is added to the Eq. (12) to make the update position of the population more reliable. The improved update position of the population is:

$$X_k(t+1) = \frac{(X_1(t+1))^2 + (X_2(t+1))^2 + (X_3(t+1))^2}{3 \sum_{i=1,2,3} X_i(t+1)} \quad (i=1,2,3) \quad (13)$$

In the position update of Eq. (13) based on weight, this paper introduces the strategy of Levy flight method. In order to ensure the search efficiency in the iterative process, the principle of greedy algorithm is used to compare the fitness values of Eq. (13) and (14), and the individual with better fitness is used as the final update position.

$$X_k(t+1) = L_v(X_\alpha(t) - X_k(t)) + X_k(t) \quad (14)$$

Where, $X_k(t+1)$ is the grey wolf individual position updated by the Levy flight method, and L_v is the flight step length, which is defined as:

$$L_v = \frac{u}{|v|^{1/\beta}} \quad (15)$$

Where, u and v are normally distributed. $u \sim N(0, \sigma_u^2)$, $v \sim N(0, 1)$. σ_u is defined as:

$$\sigma_u = \left\{ \frac{\Gamma(1+\beta) \sin(\beta\pi/2)}{2^{(\beta-1)/2} \Gamma((1+\beta)/2) \beta} \right\} \quad (16)$$

Where, β is usually taken in the range [0,2] and is taken as 1.5 in this paper, so $\sigma_u = 0.58$.

B. Polarization gradient field ambiguity correction with binocular and TOF fusion

In the process of polarization imaging, more dimensional information can be obtained compared with the ordinary image, and the zenith angle θ and azimuth angle ϕ of the surface can be obtained through the polarization information in the collected polarization image, and then the normal vector parameters of the surface can be obtained. Therefore, the reconstruction result of polarization 3D reconstruction is not related to the amount of texture on the surface of the object, and has certain advantages for low-texture objects, and can effectively avoid the disadvantage that binocular 3D reconstruction depends on texture information. In polarized vision, as shown in Fig.7, zenith angle θ is the angle between the surface normal of the target object and the centerline of the camera optical axis, and azimuth angle ϕ is the angle between the surface normal of the target object projected onto the image coordinate system plane and the clockwise direction of the positive x-axis of the image coordinate system. The gradient field is composed of surface normal calculated from zenith and azimuth angles.

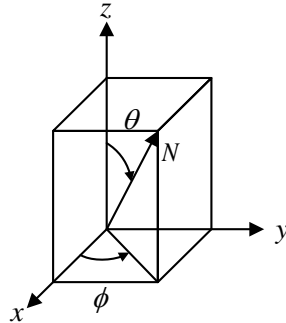


Fig.7 Schematic diagram of polarization zenith angle and azimuth angle

Common staircase materials such as concrete, wood, stone, etc. have relatively rough surfaces and many uneven structures at the microscopic level. According to the principle of reflection, when light shines on these rough surfaces, it will scatter in all directions, forming diffuse reflection. In practical environments, stairs are often illuminated by light from multiple directions, such as natural light entering through windows

or indoor lighting shining from different angles. These nonunidirectional light rays will generate complex reflections on the surface of the stairs, further increasing the proportion of diffuse reflections. Because the characteristic of diffuse reflection is the ability to uniformly reflect light at different angles and directions, diffuse reflection is easier to observe and capture under the illumination of multi-directional light. The imaging devices commonly used to obtain staircase images, such as cameras, have relatively fixed viewing angles, making it difficult to capture a specific angle that can capture a large amount of specular reflections. And diffuse reflection can be observed well from various angles, so the camera is more likely to capture the image information formed by diffuse reflection. Even though some specular reflections may be observed at certain specific angles, due to the complexity and unevenness of the staircase surface, these specular reflections are often local and incomplete, and their proportion in the entire image is still relatively small compared to large-area diffuse reflections.

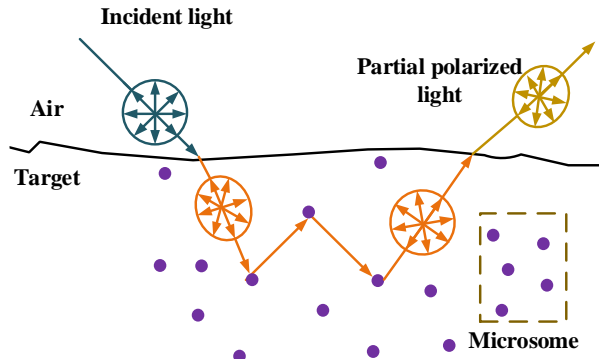


Fig.8 Schematic diagram of diffuse reflection

In this article, for the sake of analysis, it is assumed that the reflected light on the target surface is mainly diffuse reflection. As shown in Fig.8, the diffuse reflection light on the surface of an object is the component of light that enters the interior of the object through the surface and is scattered by internal particles before being refracted back into the air. The azimuth angle ϕ is:

$$\phi = \frac{1}{2} \tan^{-1} \left(\frac{s_2}{s_1} \right) \quad (17)$$

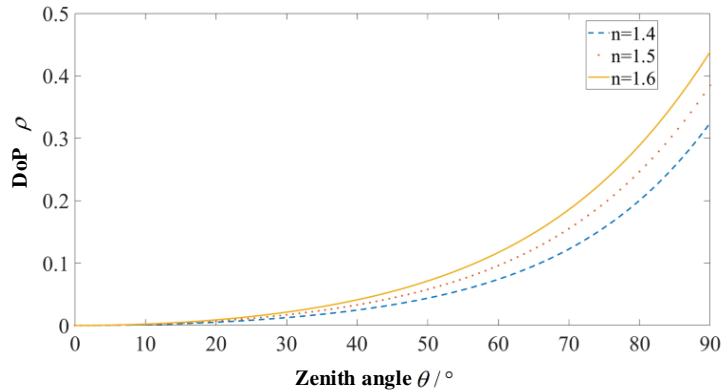


Fig.9 Schematic diagram of the relationship between DoP and zenith angle in diffuse reflection model

Another method of obtaining azimuth angle ϕ is to adjust the angle of the polarizer by rotating it. The default polarization angle ϕ at which the light intensity value reaches its peak for the first time during rotation is considered as the azimuth angle ϕ . Due to the interval range of azimuth angle ϕ being $[0, 2\pi]$ and the interval range of polarization angle being $[0, \pi]$, there is ambiguity in the solution of azimuth angle

ϕ , and the result of azimuth angle is $\phi = \varphi$ or $\phi = \varphi + \pi$.

Due to the manual operation required for the rotation process of the polarizer, there are certain errors in the rotating mechanical structure and experimental equipment. Therefore, the polarization images in this article were obtained through a polarization camera. Combining Fresnel theory, the functions of DoP ρ and zenith angle θ can be determined [32-35]:

$$\rho = \frac{(n-1/n)^2 \sin^2 \theta}{2 + 2n^2 - (n+1/n)^2 \sin^2 \theta + 4 \cos \theta \sqrt{n^2 - \sin^2 \theta}} \quad (18)$$

Where n represents the reflection coefficient. The exact value of zenith angle can be obtained by solving Eq. (18). As shown in Fig.9, Eq. (18) is a monotonic function, therefore, there is no zenith angle ambiguity in the diffuse reflection model. Based on the above analysis, in the process of 3D reconstruction of diffuse reflection polarization, there are the problems of polarization azimuth ambiguity and the noise of polarization gradient field in the case of low zenith angle, so binocular stereo vision is introduced into the 3D reconstruction of polarization to correct the polarization gradient field preliminarily. Then the 3D information of TOF is used for local correction. The specific correction scheme is shown in Fig.10.

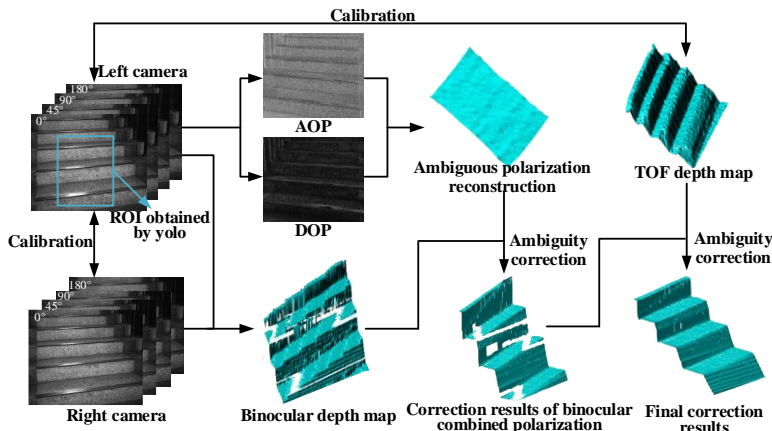


Fig.10 Polarization gradient field ambiguity correction process

The first stage is the acquisition of binocular depth images of the ROI obtained by staircase recognition. The left and right images are captured by binocular polarization camera, and then the binocular depth map is obtained by binocular imaging method. The second stage is the acquisition of the polarization depth image, the zenith angle and the azimuth angle are obtained by using the polarization image acquired by the polarization camera, the polarization gradient field is calculated according to the zenith angle and the azimuth angle, the azimuth angle ambiguity of the gradient field is corrected through the binocular depth image, and then the surface relative height of the gradient field is calculated by using the integral method. In the third stage, the normal vector of the polarization gradient field in the hole area of the binocular depth map is corrected by the normal vector of the depth map collected by the TOF camera to correct the ambiguity of the local polarization gradient field.

The zenith angle θ and azimuth angle φ of the object surface can be obtained according to the polarization imaging, so the normal vector $N^P = [N_x^P, N_y^P, N_z^P] = [\tan \theta \cos \varphi, \tan \theta \sin \varphi, 1]$ of the object surface can be obtained according to the polarization characteristics:

Obtaining the surface normal $N^B = [N_x^B, N_y^B, N_z^B]$ of the binocular depth image through the difference approximate derivative.

Comparing the polarization normal N^P with the binocular normal N^B . N^P will become the negative value of the true normal vector due to the 180° ambiguity of the azimuth angle, while the binocular normal N^B is obtained from the rough depth map through the differential approximate derivative, and the direction is correct. Therefore, the polarization normal vector N^P can be corrected by the binocular normal vector N^B . The optimization goal Λ^* can be established as:

$$\Lambda^* = \arg \min_{i \in R_1} [(N_{xi}^P - \Lambda_i \cdot N_{xi}^B)^2 + (N_{yi}^P - \Lambda_i \cdot N_{yi}^B)^2]^{1/2}, \Lambda_i \in \{-1, 1\} \quad (19)$$

Where, R_1 represents the binocular normal vector region.

Although the polarization gradient field is corrected for azimuth ambiguity by binocular depth information, there will be some low-frequency information missing in the binocular imaging process, which will lead to the binocular depth map hole. For the uncorrected normal vector corresponding to the hole region, the fusion TOF method is introduced in this paper. Firstly, the 3D information acquired by the TOF is converted into an extrinsic parameter matrix through joint calibration, and the reference coordinate system of the extrinsic parameter matrix is set as the camera coordinate system of the left camera, and the extrinsic parameter matrix is converted into a depth map, and the normal vector N^T corresponding to the depth map is obtained through derivation, and the direction of the normal vector is correct. Secondly, the hole region in the binocular depth map is obtained through the Canny algorithm, and the normal vector corresponding to the area is extracted from the TOF depth map. Therefore, the polarization normal vector N^{Ph} in the hole region can be corrected by the TOF normal vector N^T . The optimization goal Λ^{**} can be established as:

$$\Lambda^{**} = \arg \min_{i \in R_1} [(N_{xi}^{Ph} - \Lambda_i \cdot N_{xi}^T)^2 + (N_{yi}^{Ph} - \Lambda_i \cdot N_{yi}^T)^2]^{1/2}, \Lambda_i \in \{-1, 1\} \quad (20)$$

Thus, the azimuth correction of the staircase polarization information is completed. The polarization gradient field constructed by the corrected polarization normal is processed by the integral algorithm [21] to obtain the relative height of the polarization surface as shown in Fig.11.

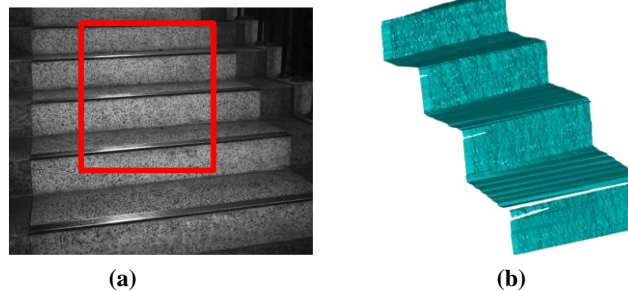


Fig.11 Polarization Gradient Field Integration Results: (a) Original image; (b) Integral results

IV. EXPERIMENT

A. Experimental equipment

The training platform used by the scene recognition algorithm is configured with Intel I5 12490F CPU, RTX 3060 GPU with 12G graphics memory, 32G storage capacity and DCAM550 TOF camera from Vzense Technology. Software used for deep learning includes Pycharm, Anaconda, and Pytorch.

The experimental platform for 3D reconstruction of polarization used in this paper consists of polarization camera, TOF camera, lens and camera holder, all of which are shown in Fig.12. The polarization camera is Daheng MER-502-79U3M-L, the resolution of the polarization angle image collected by the camera is 1024×1224 . The camera is equipped with IMX250 MZR CMOS chip and its exposure mode is global exposure. The lens is MF0828M-8 MP of Hikrobot. The TOF camera and the TOF camera used in the scene recognition algorithm are of the same model, both of which are DCAM550 produced by Vzense Technology. The camera

bracket is a self-designed rigid device to fix the relative position between the polarization camera and the TOF camera. The length of the binocular baseline constructed by the polarization camera is 50mm, and the total weight of the verification platform is 549g.



Fig.12 experimental platform for 3D reconstruction

B. Robot staircase recognition experiment

Dataset is the basis of deep learning model training. The current staircase dataset is ExoNet dataset from Laschowski team in Canada [22]. In order to ensure that the dataset conforms to the architectural style of our country and adapts to the recognition of domestic staircase, it is necessary to collect proprietary image data. Therefore, on the basis of the existing part of the data set, some self-collected staircase images are added as a supplement. The collection areas are from streets, shopping malls, schools, etc., including images of stairs with different lighting conditions, foreign body overlays, and different architectural styles. A subset of the images in the dataset is shown in Fig.13. The final training data set contains 16453 images containing the scene of staircases. The training results of the above models are shown in TABLE I.

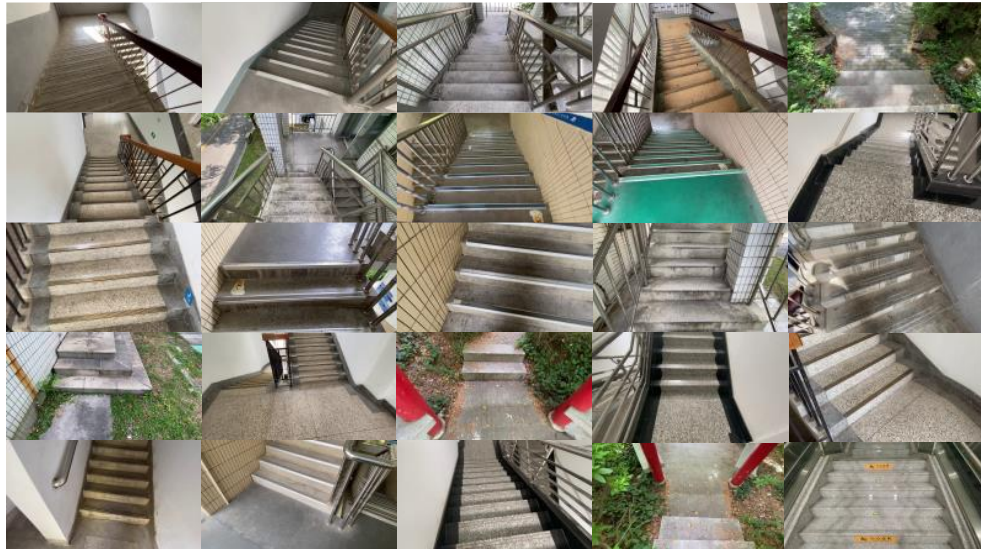


Fig.13. Schematic diagram of the images in part of the datasets

The comparison in TABLE I. proves the feasibility of our improvement on the network. The recognition performance of the improved recognition algorithm fused with 3D information is significantly improved. Compared with YOLOv11, the accuracy and frame rate are increased by 3.7%. The final recognition result is shown in Fig.14. It can be seen that the algorithm proposed in this paper can accurately generate the bounding box of the target object. And the confidence evaluation of the scene recognition results is given.



Fig.14 Scene recognition results: (a) Downstairs; (b) Upstairs

TABLE I COMPARISON OF RECOGNITION ALGORITHM RESULTS

Model	mAP(%)
YOLOv5s	96.2%
YOLOv5-Lite	92.5%
YOLOv7	96.3%
SSD	98.2%
Faster-RCNN	87.8%
Point cloud segmentation	96.7%
YOLOv11	97.1%
The algorithm proposed in this paper	98.7%

C. Experimental of joint calibration

The joint calibration method for ICP registration based on the improved grey wolf optimization algorithm can reduce the mismatching generated during the registration of the ICP algorithm. The corner points of the calibration plates under the public view of the two cameras have a corresponding relationship in the point cloud without the interference of the point cloud noise. The improved grey wolf optimization algorithm introduced to the ICP algorithm further improves the calibration precision.

The checkerboard selected in this paper is a 12×9 calibration plate with a unit length of 10 mm. The images of the calibration plate collected by the polarization camera and the TOF camera.

Firstly, the internal parameter calibration of the polarization camera and the TOF camera is completed by using the traditional calibration method to obtain the internal parameter matrix and the radial distortion coefficient of the camera, and the internal parameter matrix of the TOF camera can be obtained as follows:

$$\mathbf{K}_p = \begin{bmatrix} 456.4448 & 0 & 336.2882 \\ 0 & 457.1441 & 252.9748 \\ 0 & 0 & 1 \end{bmatrix} \quad (21)$$

The calibration result of the internal reference matrix of the polarization camera is:

$$\mathbf{K}_q = \begin{bmatrix} 1846.2992 & 0 & 604.0391 \\ 0 & 1846.9653 & 518.9741 \\ 0 & 0 & 1 \end{bmatrix} \quad (22)$$

Using the joint calibration algorithm proposed in this paper, the rigid transformation matrix between the polarization camera and the TOF camera is calculated as:

$$[\mathbf{R}, \mathbf{T}] = \begin{bmatrix} 1 & 0.0007 & 0.007 & -91.0947 \\ -0.0007 & 1 & -0.0016 & 16.5543 \\ -0.007 & 0.0016 & 1 & -22.8737 \end{bmatrix} \quad (23)$$

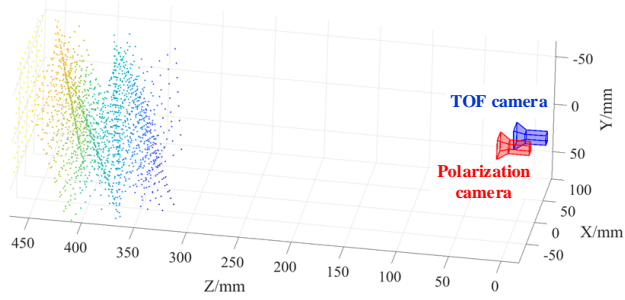


Fig.15 Schematic diagram of the point cloud distribution of the camera and calibration plate

$[R, T]$ is the relative pose relationship between the TOF camera and the polarization camera, and the schematic diagram of the relative pose relationship between the collected angular point cloud and the camera is shown in Fig.15, The result of the registration using the rigid transformation matrix between the polarization camera and the TOF camera is shown in Fig.16. By calculating the reprojection error, the calibration accuracy of this algorithm is 0.33mm.

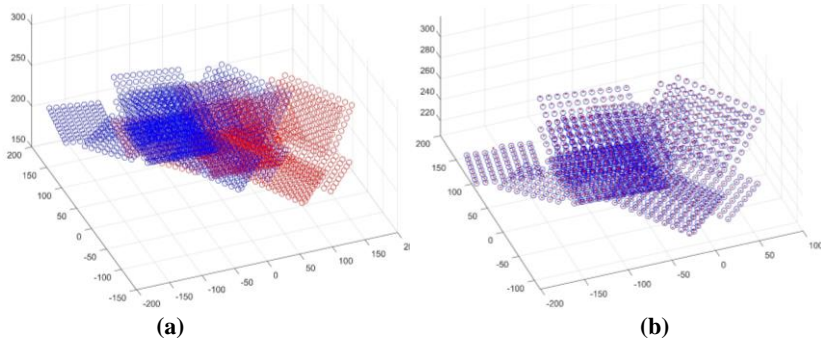


Fig.16 Schematic diagram of the registration results: (a) Before registering the calibration board corner point cloud; (b) After registering the calibration board corner point cloud

D. Staircase positioning experiment

1) Resolution analysis of scene reconstruction

The accuracy evaluation of 3D reconstruction based on binocular polarization and TOF is mainly based on the angle of reconstructed depth map. The reconstruction of the staircase mainly involves reconstructing the angle of the staircase steps. Therefore, for the measurement of this parameter, V-shaped plates are selected as auxiliary verification instruments to verify the accuracy of 3D reconstruction, in which the angles of V-shaped plates are 30 degrees, 60 degrees and 90 degrees respectively. V-shaped plates are made of light-cured resin. The machining accuracy is 0.1mm, and it is placed 0.5m away from the camera.

Fig.17(b) shows the reconstruction of the V-plate in Fig.17(a). It can be seen from the figure that the reconstruction result of the V-shaped plate is relatively flat, and the reconstructed topography is close to the real object surface, which indicates that the algorithm in this paper can effectively correct the surface gradient field of the target object. Fig.17(c) shows the depth distribution at different cross sections on the V-shaped plate at different angles. From the data in the figure, it can be seen that the distribution of the reconstructed depth deviates from the ideal value in the middle of the V-shaped plate. There are two reasons for this. The first reason is that the position of the slit is larger than the position of the polarization camera, which leads to a larger zenith angle and is vulnerable to large noise. In addition, the slit is the inflection point of the gradient field distribution, and the slit is the intersection of the gradient fields in two directions, which will cause distortion of the reconstruction results.

Fig.17(c) shows the distribution between the target section depth and the ideal depth of the V-shaped plate.

From the image, it can be seen that the distribution trend between the target section depth and the ideal depth in Fig.17(a) is consistent. Because the polarization gradient field is calculated by the polarization optical information, it is inevitable that there will be data errors and noise in the data acquisition process. The result of the polarization gradient field can only be approximated by the gradient field without noise and error, and can not be absolutely equal.

According to the ideal depth map, the linear equation $ax + by + c = 0$ is fitted, and the error between the ideal depth and the actual depth is calculated by subtracting it from the actual reconstruction depth value. Based on this, the average and maximum errors of the 90° V-shaped plates are 0.46mm and 1.02mm, respectively. The ratio of the maximum reconstruction error to the target distance is $\alpha = \frac{1.02}{500} \times 100\% \approx 0.2\%$. Among them, due to the small zenith angle at the middle edge of the V-shaped plate, there is significant noise and errors at this location.

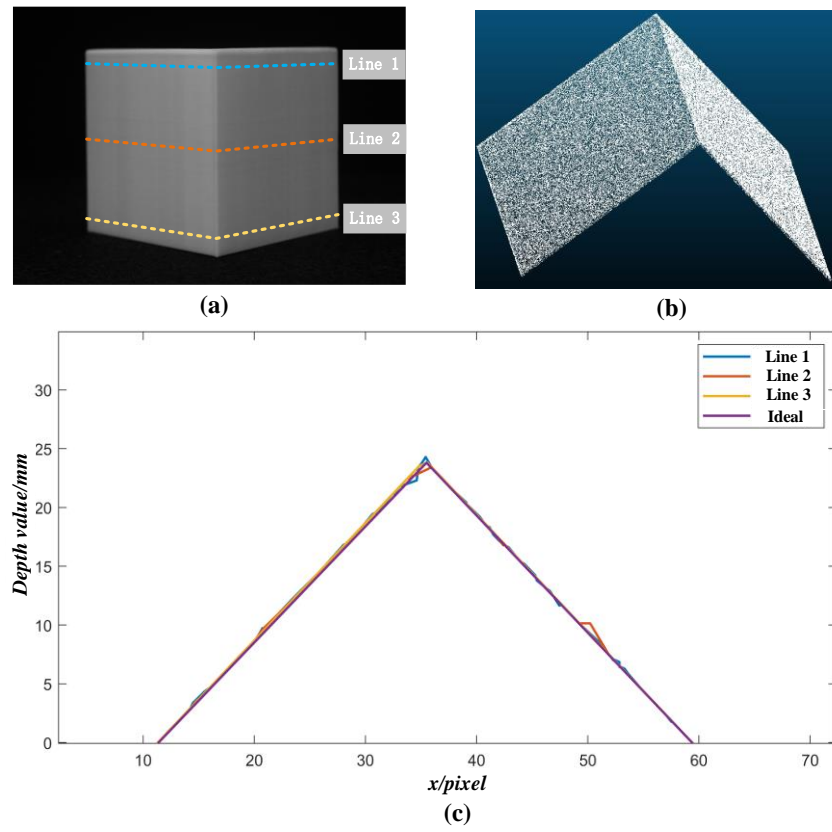


Fig.17 90° V-plates reconstruction result

2) Comparison of Reconstruction Results

The 3D reconstruction effect of integrating binocular polarization and TOF proposed in this paper is shown in Fig.18. The method proposed in this paper has been compared with polarization reconstruction [23], binocular reconstruction [24], monocular polarization fusion depth sensor [25], and binocular polarization fusion photometric stereo [13]. The experimental object selected in this paper is the staircase.

As shown in the reconstruction results in the figure, due to the lack of correction for gradient field ambiguity in polarization 3D reconstruction, the reconstruction results did not show the correct trend of scene morphology, presenting an overall plane. As shown in Fig.19, compared with several algorithms with relatively good reconstruction results, the algorithm in this paper portrays the details better. Specifically, its reconstruction results are closer to the object features of stairs in actual scenes, the surface is smoother, and the reconstruction distortion is smaller.

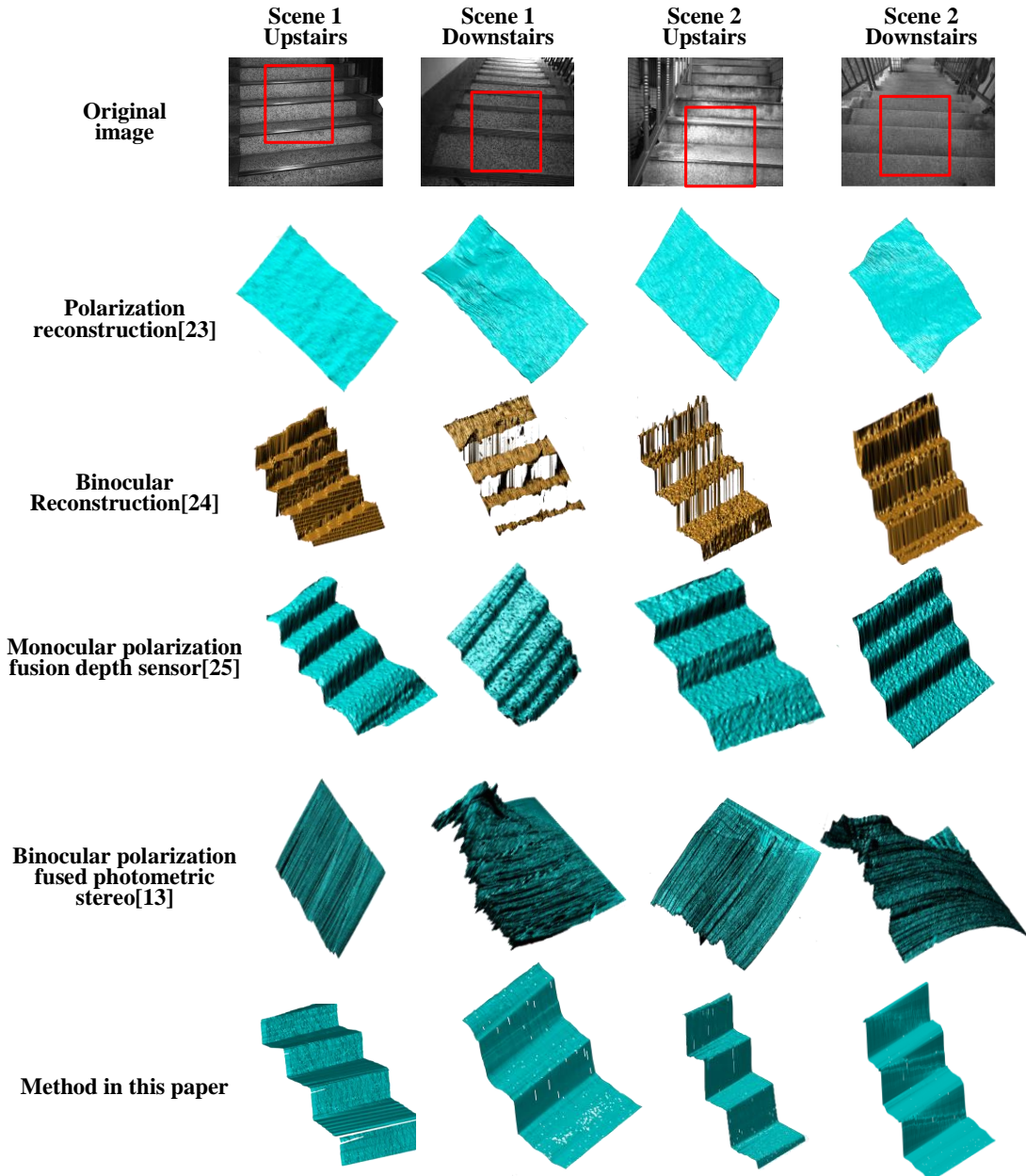


Fig.18 Comparison of polarization 3D reconstruction results

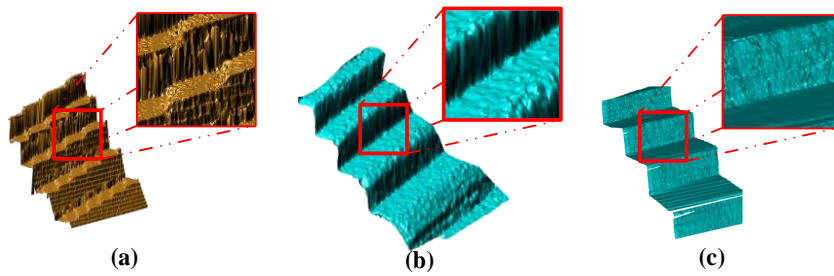


Fig.19 The results of the reconstruction and their details are displayed: (a) Binocular reconstruction; (b) Monocular polarization fusion depth sensor; (c) Reconstruction proposed in this paper

Polarization 3D reconstruction results in significant distortion due to ambiguity in the direction of normal vectors, making it difficult to accurately obtain the reconstructed target morphology. Although the method

of binocular 3D reconstruction can obtain a relatively correct morphology of the object surface, the details of the reconstruction results are poor and the surface is uneven due to matching errors, noise, and other effects in the stereo matching process. TOF imaging is sensitive to light due to time resolution. Under the influence of multipath effects and time resolution, the echo signal is prone to phase delay and noise during reception, resulting in significant reconstruction errors. The surface potholes in the reconstruction results are a manifestation of reconstruction errors. The binocular polarization fusion photometric stereo method requires early calibration of the light source position direction, and the outdoor environment cannot achieve accurate calibration of the light source position. The limitations of the photometric stereo algorithm make it difficult to select structurally complex objects in the selection of reconstruction targets. Therefore, it is difficult to achieve high-quality staircase reconstruction in outdoor environments.

V. DISCUSSION

This paper mainly studies the perception of staircase scenes based on polarization 3D vision. A system combining scene recognition, 3D reconstruction, and point cloud processing is designed to improve recognition accuracy. Polarization vision can obtain more dimensional information than ordinary RGB or grayscale images. In reality, 3D reconstruction is based on the polarization information of the target object surface. Therefore, the fusion of binocular polarization and TOF methods can achieve the reconstruction of staircase.

This paper first focuses on the interference of reflection on target detection, and constructs a DoP image and intensity image fusion based on MLP network to improve the contrast of the input image for object detection, and proposes a point cloud segmentation based on normal vector differences for secondary recognition to improve recognition accuracy, achieving the accuracy improvement of the staircase recognition network. Secondly, the joint calibration of monocular cameras and TOF cameras was completed. In order to obtain a relatively accurate rigid transformation matrix for high-resolution monocular cameras and low resolution TOF cameras, the ICP point cloud registration method was first used to register the spatial coordinates of the checkerboard corner points. Then, the output results were optimized using an improved grey wolf optimization algorithm combining Levy flight method and chaotic mapping, ultimately achieving high-precision calibration. Finally, the stereo polarization fusion TOF method was implemented for 3D reconstruction of staircase. This 3D reconstruction method avoids the characteristics of poor mapping details, weak anti-interference ability, and being limited by time resolution and lighting of a single sensor.

Through experimental analysis and algorithm comparison, it has been verified that the scene recognition algorithm in this paper can effectively improve detection accuracy, with an accuracy of 98.7%. Compared to using the YOLOv11 network alone, the accuracy can be improved by 3.5%. Secondly, it was verified that the joint calibration accuracy of TOF monocular cameras can reach 0.5mm. Finally, based on the TOF monocular camera joint calibration and comparison with classic reconstruction methods, binocular stereo matching, monocular polarization fusion depth sensors, and binocular polarization fusion photometric stereo methods, this method achieves more refined mapping and higher accuracy.

In future applications, the relevant technologies proposed in this paper can be applied to humanoid robots or exoskeleton robots for footstep planning in staircase scenes, achieving autonomous movement of humanoid robots in staircase scenes, or assisting exoskeleton robots in the field of elderly and disability assistance to help target populations traverse staircase scenes as redundant information. At present, the control of exoskeleton robots is mostly based on electromyographic signal sensors, which rely more on human motion intentions and lack the ability to perceive the scene. The introduction of visual information greatly enhances the perception ability of the scene. The fusion of photoelectric sensors and wearable sensors can further determine whether the best foot point exists in front of the current motion scene. As shown in

Fig.20 and 21, the landing point planning in the staircase scene and the walking trajectory of the exoskeleton robot after introducing visual information on the staircase are shown. Due to the low robustness of the algorithm, filtering the noise that exists after segmentation leads to inconsistent step heights in the staircase scene in Fig.20. In future practical use, the segmentation algorithm still needs to be optimized.

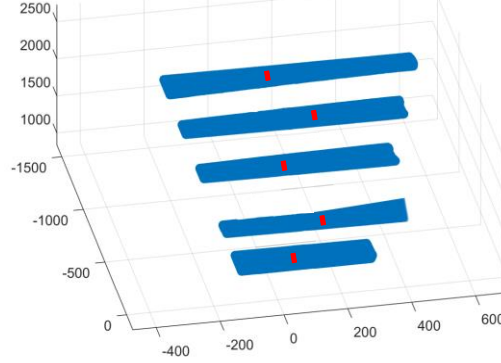


Fig.20 Robot landing point path planning

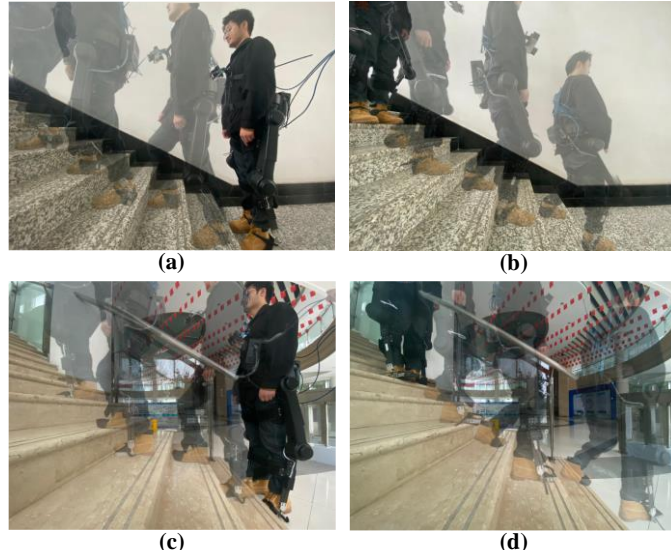


Fig.21 Robot motion trajectory: (a) Scene 1: Going up the stairs; (b) Scene 1: Going down the stairs; (c) Scene 2: Going up the stairs; (d) Scene 2: Going down the stairs

This study focuses on the perception of staircase scenes based on polarized 3D vision, but there is still a significant gap with the actual application goals. Therefore, there are still some issues that need further research in this study:

- (1) The target scenario targeted in this paper is relatively single, and only experiments were conducted on the staircase scenario. In the future, it is necessary to expand the target scenario, such as slopes, puddles, and shallow ditches, to achieve the universality of the algorithm.
- (2) This paper involves a wide variety of sensors, making it inconvenient for robots to carry. In the future, lightweight hardware selection should be carried out while ensuring hardware performance. Moreover, the fusion of multiple sensors requires high computational power and is difficult to embed into resource limited computer devices. In the future, while ensuring performance, complexity should be effectively reduced. Hardware acceleration and parallel processing of feature extraction and classification recognition can effectively alleviate the computational pressure brought by multi-sensor data fusion to the system.

(3) This paper only perceives the staircase scene from the perspective of computer vision, and the use of information sources is relatively single. In the future, user perception and sensor recognition can be integrated to achieve more intelligent technology, avoiding ignoring the possibility of human consciousness conflicting with the instructions issued by the system during movement. In addition, the fusion of user perception and sensor recognition makes this technology more intelligent. When the photoelectric sensor recognizes the terrain that is about to move, it switches the motion gait. Wearable sensors are used to detect whether the gait meets the requirements for moving on the staircase.

VI. CONCLUSION

Due to the low scene recognition rate, high computational requirements for recognition algorithms, susceptibility to environmental light interference, and avoidance of texture dependence on target objects during robot traversal in staircase scenes, this paper proposes a staircase recognition and 3D reconstruction method that integrates polarized binoculars and TOF. In terms of staircase recognition, the accuracy of staircase scene recognition is improved by fusing DoP image and intensity image to improve the contrast of the input image and integrating 3D point cloud information. In terms of 3D reconstruction of staircase, the introduction of polarization method reduces the interference of ambient light and the dependence on object surface texture. The fusion with binocular vision and TOF reduces data holes in the reconstruction results, and corrects the problem of normal vector ambiguity in the polarization gradient field. In the fusion process of binoculars and TOF, this paper also proposes an improved grey wolf optimization algorithm for joint camera calibration. Compared with existing methods, the method proposed in this paper has higher recognition accuracy, relatively high calibration accuracy, and better texture details in the reconstructed results.

This work was supported by National Key R&D Program of China (2023YFB3907203), Key R&D Plan of Jiangsu Province (BE2020082-1 and BE2021016-4), Fundamental Research Funds for the Central Universities (B230201005) and Anhui Provincial Natural Science Foundation (1808085QF193).

REFERENCES

- [1] G. Lin, X. Zhao, W. Wang and T. Wilkinson, "The relationship between forward head posture, postural control and gait: A systematic review," *Gait & Posture*, vol. 98, Oct. 2022, pp.316-329.
- [2] J. Zhu, F. Li, H. Li and D. Zhai, "Design and Motion Analysis of Wheel-legged Step-climbing Mobile Robot," *Chin. J. Mech. Eng.* vol.24, no.20, Aug. 2013, pp. 2722-2730.
- [3] C. Chen, J. Leng, Q. Li, Y. Hou, T. LÜ. "A Stair-climbing Gait of a Multi-mode Omni-directional Mobile Robo," *ROBOT*, vol.44, no.4, Jun. 2022, pp. 453-462.
- [4] Q. Guo, W. Guo, D. Wang, J. Cheng and X. Liu, "Multi-stage Motion Denoising Network with Multimodal Fusion of Kinect and IMU Data," *J. Chin. Comput. Syst.* vol.45, no.1, Jan.2024, pp.16-22.
- [5] D. Dong, C. Ma, M. Wang, H. T. Vu, B. Vanderborght, Y. Sun, "A low-cost framework for the recognition of human motion gait phases and patterns based on multi-source perception fusion," *Eng. Appl. Artif. Intell.* vol.120, Apr. 2023, Art. no. 105886.
- [6] E. Lattanzi and V. Freschi, "Evaluation of human standing balance using wearable inertial sensors: A machine learning approach," *Eng. Appl. Artif. Intell.* vol.94, Sep. 2020, 103812.
- [7] B. Vidya and P. Sasikumar, "Parkinson's disease diagnosis and stage prediction based on gait signal analysis using EMD and CNN-LSTM network," *Eng. Appl. Artif. Intell.* vol.114, Sep. 2022, 105099.
- [8] W. Kong, Z. Tan, W. Fan, X. Tao, M. Wang, L. Xu and X. Xu, "A Review of the Application of Staircase Scene Recognition System in Assisted Motion," *Digit. Signal Process.* vol.146, Mar. 2024, 104362.
- [9] X. Xu, Z. Fei, Z. Tan, B. Zhao, and J. He, "Improved calibration method based on the RANSAC approach and an improved gray centroid method for a laser-line-based structured light system," *Appl. Opt.* vol.58, Dec. 2022, pp. 9603–9613.
- [10] Z. Tan, W. Kong, Y. Ji, X. Tao, J. Zhao, M. Wang, and X. Xu, "Shape recovery from fusion of polarization binocular vision and shading," *Appl. Opt.* vol.62, Aug. 2023, pp. 6194-6204.
- [11] F. Liu, S. Sun, P. Han, K. Yang and X. Shao, "Development of Underwater Polarization Imaging Technology," *Laser Optoelectron. P.* vol.58, no.6, Mar. 2021, 060001.
- [12] X. Li, Z. Liu, Y. Cai, C. Pan, J. Song, J. Wang and X. Shao, "Polarization 3D imaging technology: a review," *Front. Phys.* vol.11, May. 2023, 1198457.
- [13] Z. Tan, B. Zhao, Y. Ji, X. Xu, Z. Kong, T. Liu, and M. Luo, "A welding seam positioning method based on polarization 3D reconstruction and linear structured light imaging," *Opt. Laser Technol.* Vol.151, Jul. 2022, 108046
- [14] R. Zou, Y. Zhang, J. Gu, and J. Chen, "Simultaneous measurement of 3D surface and thickness of large area and thickness transparent materials based on polarization model and TOF correction," *Optik*, vol.254, Mar. 2022, 168560

- [15] X. Li, F. Liu, P. Han, S. Zhang, and X. Shao, “Near-infrared monocular 3Dcomputational polarization imaging of surfaces exhibiting nonuniform reflectance,” Opt. Express. Vol.29, May. 2021, pp. 15616–15630.
- [16] P. Han, Y. Cai, F. Liu, X. Li, R. Liang, M. Yan, and X. Shao, “Computational 3D: new solution for monocular shape recovery in natural conditions,” Opt. Laser Eng. vol. 151. 2022. 106925
- [17] Y. Huang and F. Da, “Three-dimensional face point cloud hole-filling algorithm based on binocular stereo matching and a B-spline”, Frontiers of Information Technology & Electronic Engineering, vol.23, no.3, Mar. 2022, pp. 398-408.
- [18] X. Wang, W. Zhou and Y. Jia, “Attention GAN for Multipath Error Removal From ToF Sensors”, IEEE Sens. J. vol. 22, no.20, Oct. 2024, pp.19713-19721.
- [19] Z. Zhang, “A Flexible New Technique for Camera Calibration,” IEEE Trans. Pattern Anal. Mach. Intell. vol.22, no.11, Nov. 2000, pp.1330-1334.
- [20] S. Mirjalili, S. M. Mirjalili, A. Lewis, “Grey Wolf Optimizer,” Adv. Eng. Softw. vol. 69, Mar. 2014, pp.49-61.
- [21] R. T. Frankot and R. Chellappa, “A method for enforcing integrability in shape from shading algorithms,” IEEE Trans. Pattern Anal. Mach. Intell. vol.10, Aug. 1988, pp. 439–451.
- [22] B. Laschowski, W. McNally, A. Wong and J. McPhee, “Computer Vision and Deep Learning for Environment-Adaptive Control of Robotic Lower-Limb Exoskeletons,” In Proc. EMBC, Mexico, 2021, pp.4631-4635.
- [23] K. Koshikawa, “A polarimetric approach to shape understanding of glossy objects,” in Proc. IJCAI, Tokyo, Japan, 1979, pp. 190–192.
- [24] A. Fusillo, E. Trucco, and A. Verri, “A compact algorithm for rectification of stereo pairs,” Mach. Vis. Appl. vol. 12, Jul. 2000, pp.16–22.
- [25] J. Yang, L. Yan, H. Zhao, R. Chen, R. Zhang and B. Shi, “Shape from Polarization of low-texture objects with rough depth information,” J. Infrared Millim. Waves. vol.38, no.6, Dec. 2019, pp.819-827.